Electronic Supplementary Material (ESI) for Nanoscale Advances.

Ligand-assisted deposition of ultra-small Au nanodots on Fe_2O_3/reduced graphene oxide for flexible gas sensors

Jian Wang,[a] Essalhi Fatima-ezzahra,[a] Jie Dai,[a] Yanlei Liu,[a] Chengjie Pei,[a] Hai Li,[a] Zhiwei Wang*[a,b] and Xiao Huang*[a]

[a] Institute of Advanced Materials (IAM), Nanjing Tech University (Nanjing Tech), 30 South Puzhu Road, Nanjing 211816, China. E-mail: iamxhuang@njtech.edu.cn

[b] Frontiers Science Center for Flexible Electronics, Xi'an Institute of Flexible Electronics (IFE) and Xi'an Institute of Biomedical Materials & Engineering, Northwestern Polytechnical University, 127 West Youyi Road, Xi'an 710072, China. E-mail: iamzwwang@nwpu.edu.cn

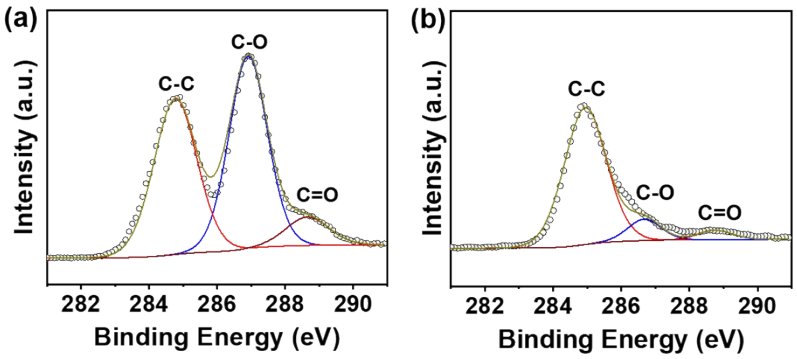

Figure S1 C 1s XPS spectra of (a) GO and (b) α-Fe_2O_3/rGO.

The C 1s XPS spectra of GO and α-Fe_2O_3/rGO are shown in Fig. S1a and S1b respectively. Three peaks at 284.6, 286.6, and 288.5 eV can be assigned to C-C, C-O, and C=O species. The peak intensities for C-O and C=O in α-Fe_2O_3/rGO were much lower than those in GO, indicating the largely removal of oxygen groups of GO during hydrothermal reaction.[1]

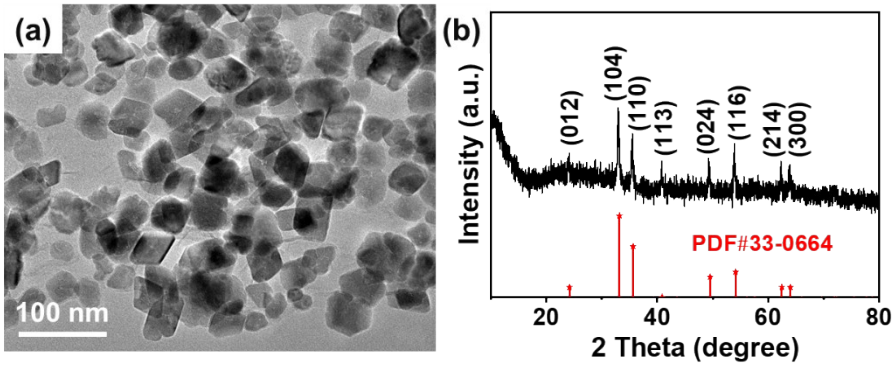

Figure S2 (a) TEM image of α-Fe_2O_3/rGO. (b) XRD pattern of α-Fe_2O_3/rGO showing mainly peaks for α-Fe_2O_3.

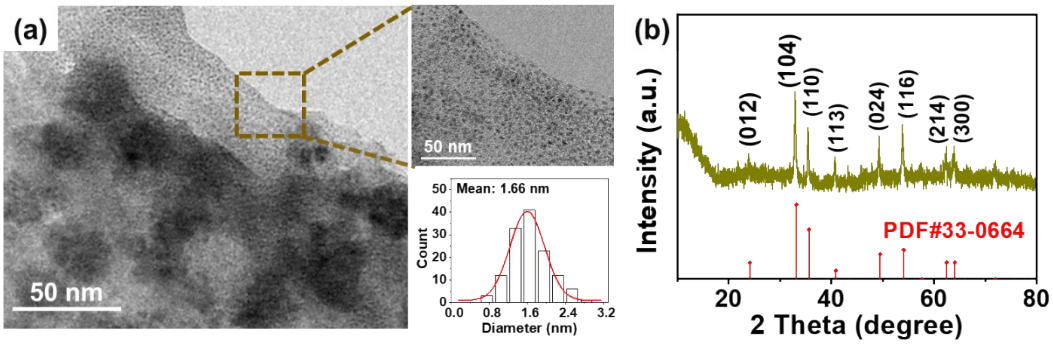

Figure S3 (a) TEM image of Au ND-ODT/α-Fe_2O_3/rGO hybrid (left) and size distribution of the Au NDs (right). (b) XRD pattern of Au ND-ODT/α-Fe_2O_3/rGO showing mainly peaks for α-Fe_2O_3.

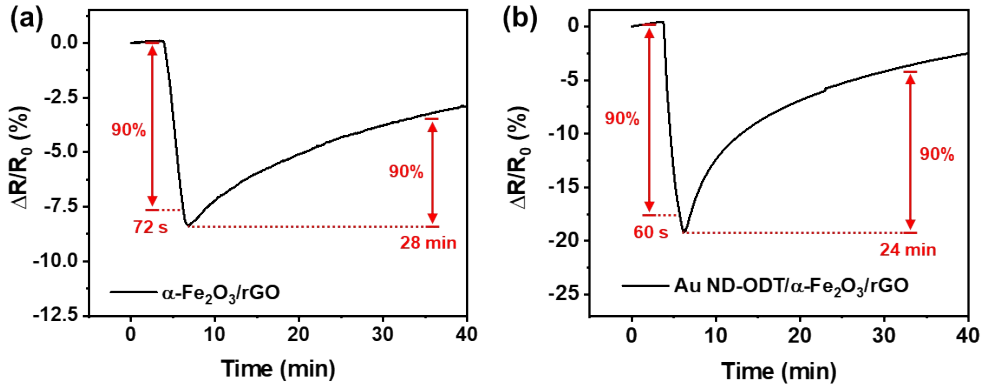

Figure S4 Dynamic response-recovery curves of (a) α-Fe_2O_3/rGO and (b) Au ND-ODT/α-Fe_2O_3/rGO to 800 ppb NO_2 gas.

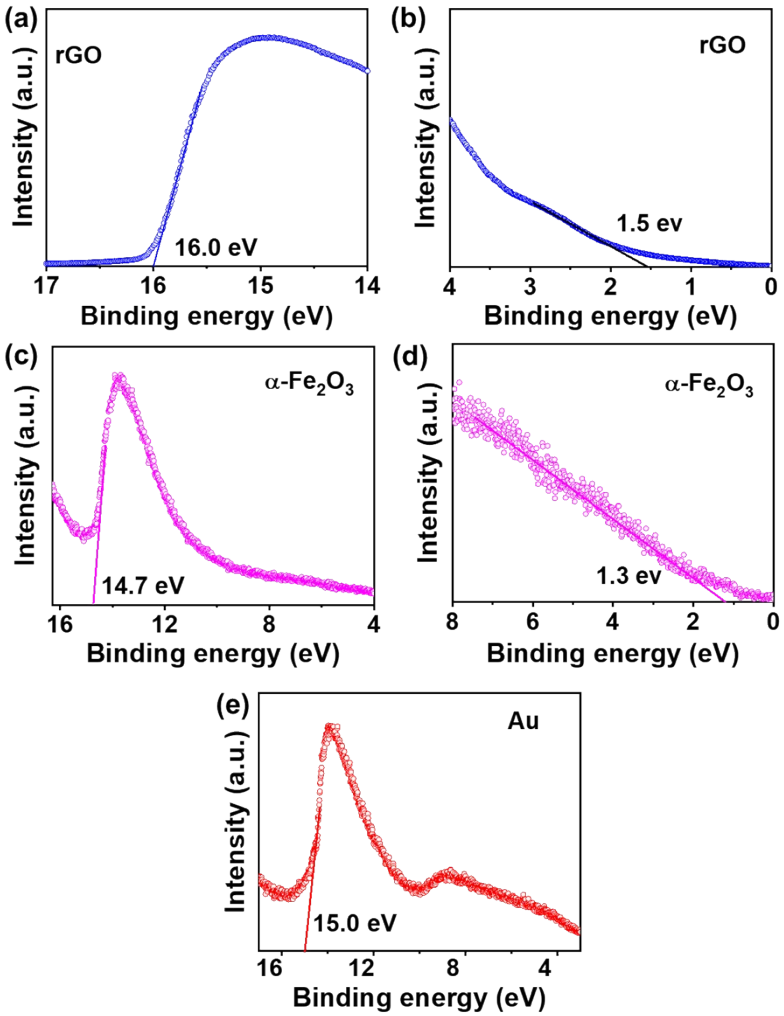

Figure S5 UPS analysis of (a, b) rGO, (c, d) α-Fe_2O_3, and (e) Au NDs.

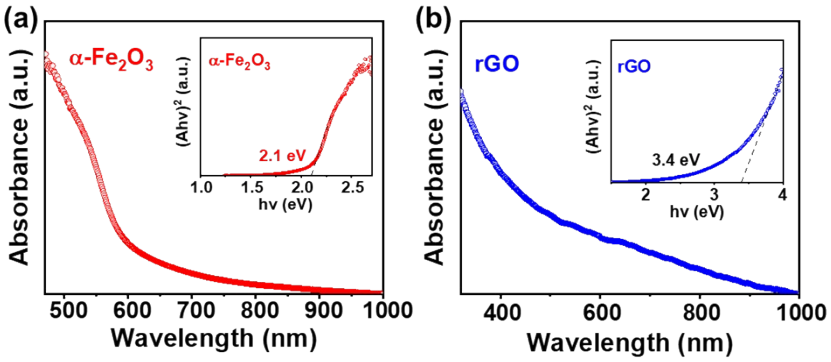

Figure S6 UV-vis absorption spectra of (a) α-Fe_2O_3 and (b) rGO. Inset: Tauc plot extrapolation for α-Fe_2O_3 and rGO.

Table S1 Comparison of the sensing performance between the recently reported room-temperature NO_2 sensors and Au ND-ODT/α-Fe_2O_3/rGO sensor.

Material	Limit of detection (ppm)	Response ($\|\Delta R/R_0\|$)	Highest response to indicated gases to show selectivity	Ref.
Au ND-ODT/α-Fe_2O_3/rGO	**0.2**	**22.5% @ 1 ppm**	**2.4% @ 1 ppm H_2S**	**This work**
rGO nanofibrous mesh	1	26.5% @ 5 ppm	1.3% @ 1 ppm C_6H_6	2
rGO nanofiber	0.25	0.8% @ 0.25 ppm	9.2% @ 10 ppm NH_3	3
polypyrrole/nitrogen-doped multiwall carbon nanotube	0.25	25% @ 5 ppm	3% @ 10 ppm H_2S	4
Ag-CuO/rGO	1	1.2% @ 1 ppm	31% @ 200 ppm H_2S	5
C-decorated SnO_2	0.5	63% @ 0.5 ppm	1.7% @ 10 ppm H_2S	6
Au-CuO	1	33.3% @ 1 ppm	35% @ 1000 ppm NH_3	7
Au NP/g-C_3N_4	0.1	2.4% @ 0.5 ppm	2.5% @ 100 ppm Hexane	8
g-C_3N_4/GaN	0.5	0.6% @ 0.5 ppm	22.5% @ 5 ppm H_2S	9
MoS_2	5	17.8% @ 5 ppm	11% @ 500 ppm NH_3	10

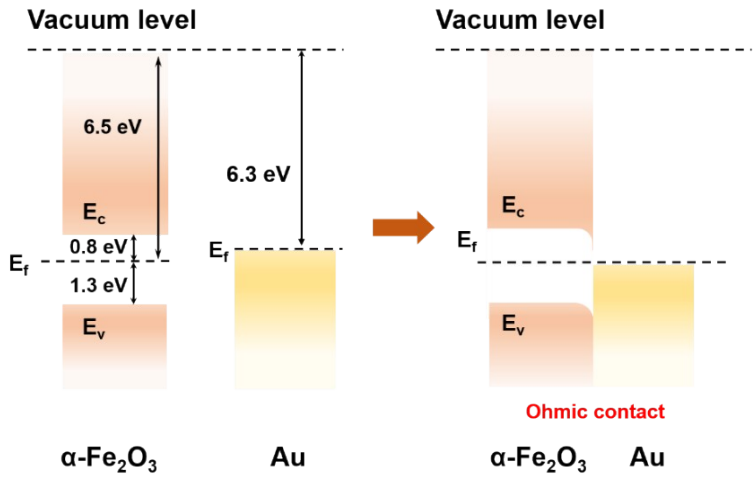

Figure S7 Schematic diagram of the band level diagram between α-Fe_2O_3 and Au NDs.

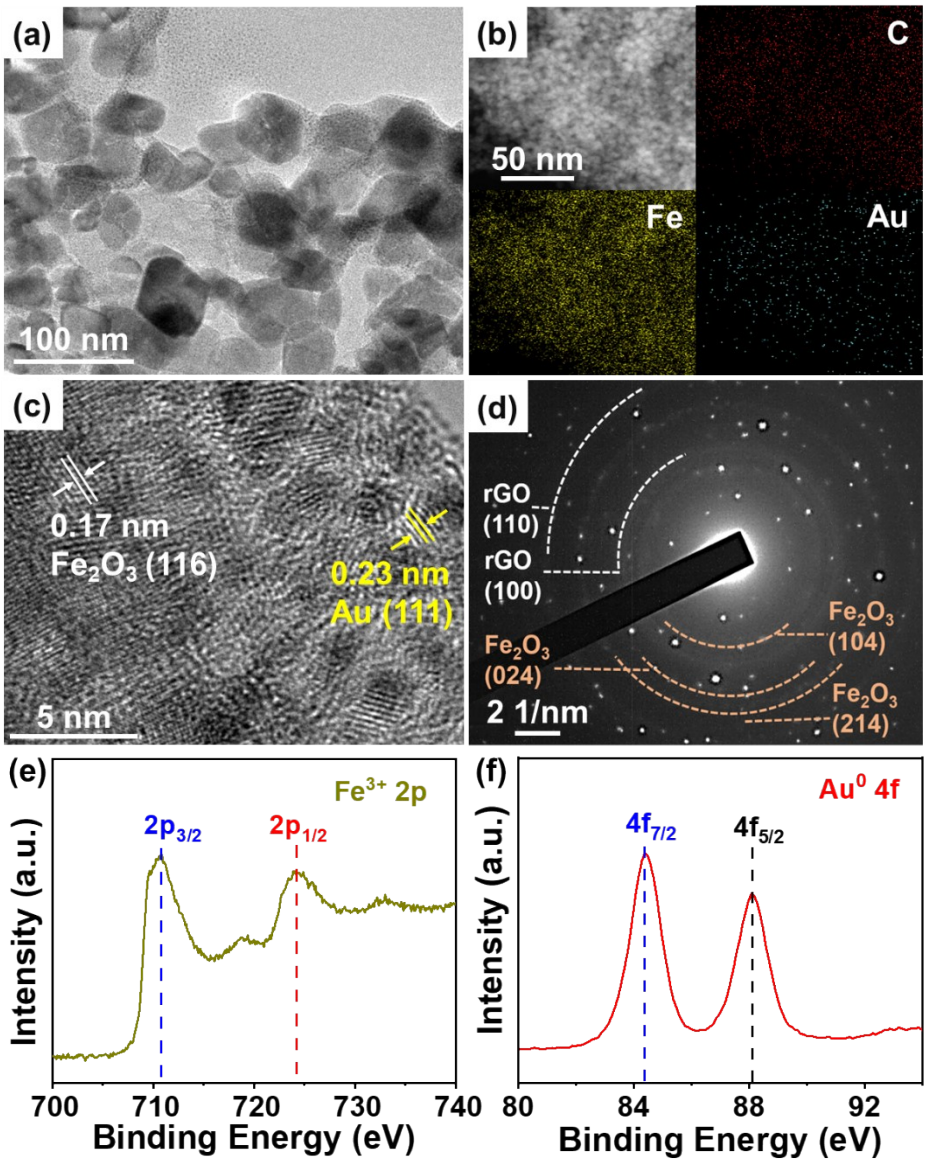

Figure S8 (a) TEM image, (b) STEM image coupled with EDX mapping, (c) HRTEM image, (d) SAED pattern, (e) high-resolution Fe 2p spectrum and (f) Au 4f spectrum of Au ND-MHA/α-Fe_2O_3/rGO hybrid.

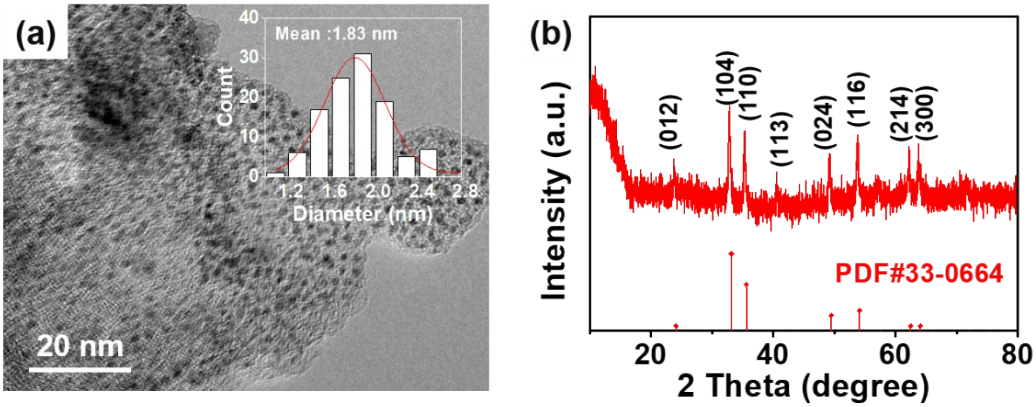

Figure S9 (a) TEM image of Au ND-MHA/α-Fe_2O_3/rGO hybrid. Inset: Size distribution of the Au NDs. (b) XRD pattern of Au ND-MHA/α-Fe_2O_3/rGO showing mainly peaks for α-Fe_2O_3.

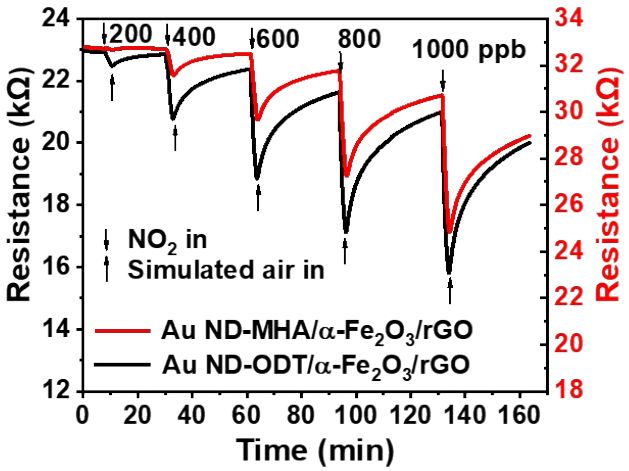

Figure S10 Dynamic response-recovery curves of sensors based on Au ND-ODT/α-Fe_2O_3/rGO hybrid and Au ND-MHA/α-Fe_2O_3/rGO hybrid in response to NO_2 gas with increasing concentration at RT.

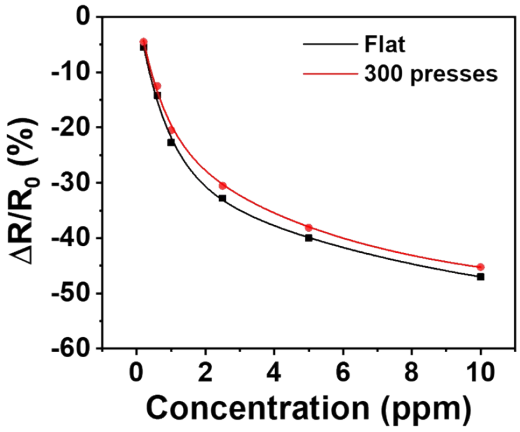

Figure S11 Comparison of the responses of a typical Au ND-ODT/α-Fe_2O_3/rGO sensor to NO_2 before and after 300 times of repeated bending at a bending angle of 30°.

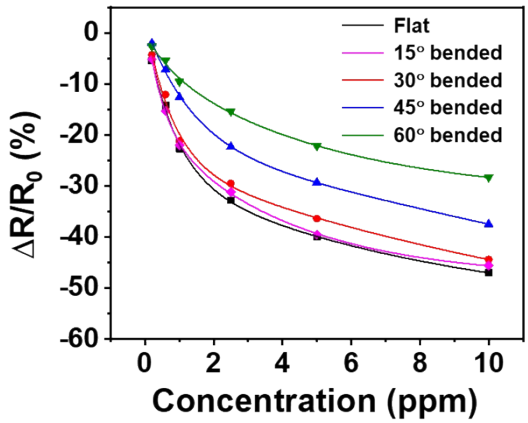

Figure S12 Comparison of the responses of a typical Au ND-ODT/α-Fe_2O_3/rGO sensor to NO_2 under flat and different bended conditions.

References

1 R. Peng, Y. Li, T. Liu, Q. Sun, P. Si, L. Zhang and L. Ci, *Chem. Phys. Lett.*, 2019, **737**, 136829-136834.

2 H. J. Park, W. J. Kim, H. K. Lee, D. S. Lee, J. H. Shin, Y. Jun and Y. J. Yun, *Sens. Actuat. B*, 2018, **257**, 846-852.

3 J. Zha, Z. Yuan, Z. Zhou, Y. Li, J. Zhao, Z. Zeng, L. Zhen, H. Tai, C. Tan and H. Zhang, *Small Struct.*, 2021, **2**, 2100067.

4 B. Liu, X. Liu, Z. Yuan, Y. Jiang, Y. Su, J. Ma and H. Tai, *Sens. Actuat. B*, 2019, **295**, 86-92.

5 Jyoti and G. D. Varma, *J. Alloys Compd.*, 2019, **806**, 1469-1480.

6 M. S. Choi, H. G. Na, J. H. Bang, A. Mirzaei, S. Han, H. Y. Lee, S. S. Kim, H. W. Kim and C. Jin, *Sens. Actuat. B*, 2021, **326**, 128801.

7 X. Chen, S. Zhao, P. Zhou, B. Cui, W. Liu, D. Wei and Y. Shen, *Sens. Actuat. B*, 2021, **328**, 129070.
8 S. Li, Z. Wang, X. Wang, F. Sun, K. Gao, N. Hao, Z. Zhang, Z. Ma, H. Li, X. Huang and W. Huang, *Nano Res.*, 2017, **10**, 1710-1719.
9 M. Reddeppa, N. T. KimPhung, G. Murali, K. S. Pasupuleti, B. G. Park, I. In and M. D. Kim, *Sens. Actuat. B*, 2021, **329**, 129175.
10 R. Kumar, N. Goel and M. Kumar, *ACS Sens.*, 2017, **2**, 1744-1752.